PHOTONICS Research

Realizing transmitted metasurface cloak by a tandem neural network

Zheng Zhen,[1,2,3] Chao Qian,[1,2,3,5] Yuetian Jia,[1,2,3] Zhixiang Fan,[1,2,3] Ran Hao,[4,6] Tong Cai,[1,2,3] Bin Zheng,[1,2,3,7] Hongsheng Chen,[1,2,3] and Erping Li[1,2,3]

[1]Interdisciplinary Center for Quantum Information, State Key Laboratory of Modern Optical Instrumentation, College of Information Science and Electronic Engineering, Zhejiang University, Hangzhou 310027, China
[2]ZJU-Hangzhou Global Science and Technology Innovation Center, Key Laboratory of Advanced Micro/Nano Electronic Devices & Smart Systems of Zhejiang, Zhejiang University, Hangzhou 310027, China
[3]International Joint Innovation Center ZJU-UIUC Institute, Zhejiang University, Haining 314400, China
[4]College of Optical and Electronic Technology, China Jiliang University, Hangzhou 310018, China
[5]e-mail: chaoqianzju@zju.edu.cn
[6]e-mail: ran.hao@cjlu.edu.cn
[7]e-mail: zhengbin@zju.edu.cn

Received 6 January 2021; revised 4 March 2021; accepted 4 March 2021; posted 12 March 2021 (Doc. ID 418445); published 30 April 2021

Being invisible at will has been a long-standing dream for centuries, epitomized by numerous legends; humans have never stopped their exploration steps to realize this dream. Recent years have witnessed a breakthrough in this search due to the advent of transformation optics, metamaterials, and metasurfaces. However, the previous metasurface cloaks typically work in a reflection manner that relies on a high-reflection background, thus limiting the applications. Here, we propose an easy yet viable approach to realize the transmitted metasurface cloak, just composed of two planar metasurfaces to hide an object inside, such as a cat. To tackle the hard-to-converge issue caused by the nonuniqueness phenomenon, we deploy a tandem neural network (T-NN) to efficiently streamline the inverse design. Once pretrained, the T-NN can work for a customer-desired electromagnetic response in one single forward computation, saving a great amount of time. Our work opens a new avenue to realize a transparent invisibility cloak, and the tandem-NN can also inspire the inverse design of other metamaterials and photonics. © 2021 Chinese Laser Press

https://doi.org/10.1364/PRJ.418445

1. INTRODUCTION

Perhaps no one feels unfamiliar with the possibility of an invisibility cloak, as this long-standing dream has been epitomized by numerous legends and novels for centuries. To realize this dream, humans have never stopped their exploration. Particularly, in the past decades, the advent of metamaterials and nanotechnology has ignited unprecedented enthusiasm in realizing manmade cloaks that brings a new twist to the conventional cloaking community [1–7]. A groundbreaking proposal of a transformation optics-based cloak renders an object invisible by bending the flow of light around it, suppressing the scattering to be exactly zero [2]. In theory, this method is perfect; however, in experiment, it is marred by the bulky material compositions with both anisotropy and inhomogeneity [3]. As the two-dimensional (2D) equivalence of metamaterials, metasurfaces recently have demonstrated their rich optical properties in providing abrupt phase shift, amplitude modulation, and polarization conversion of electromagnetic (EM) waves [8–15]. By covering a deliberately designed metasurface over the hidden object, the scattered fields can be reconstructed as if an incident wave were to impinge onto a pure background without the hidden object [16–20]. The usage of metasurface greatly reduces the thickness and complexity of invisibility cloaks, but they typically work in a reflection manner, known as a carpet cloak, and rely on a high-reflection background as the reference. This dependence limits its applications.

The transmitted metasurface cloak can properly compensate for the imperfectness of a reflected metasurface cloak and work without any background (free-standing invisibility cloak), i.e., creating an illusion of free space. Therefore, the EM wave should be either guided around the hidden object or compensated for by lossy/gain media, putting forward a higher requirement for the metasurface design. So far, there have been some proposals about transmitted metasurface cloaks; for example, Ref. [21] integrated transparent metasurfaces and zero-index materials together to realize a hybrid invisibility cloak in transmission geometry; Ref. [22] proposed a parity-time symmetric metasurface with balanced gain and loss to realize a cloak in a particular direction. These works greatly enrich the transmitted

metasurface cloak, but they are complicated and cumbersome in practical implementation. Also, in designing these cloaks, the key step—metasurface design—conventionally relies on time-consuming EM numerical simulations, assisted by manual fine-tuning or optimization algorithms, such as genetic algorithms, to iteratively approach the demanded optical responses. Fundamentally, these stochastic algorithms work in a trial-and-error manner that are limited by their random search nature [23–30]. Given these factors, albeit challenging, a practical preferable transmitted metasurface cloak approach and an intelligent design algorithm have been highly sought after.

In this paper, an easy yet viable approach is proposed to realize the transmitted metasurface cloak, and a tandem neural network (T-NN) to efficiently streamline the inverse design process is introduced. The transmitted metasurfaces cloak is composed of two planar metasurfaces to hide an object inside, such as a cat. Compared with conventional methods, our transparent cloak does not involve any active component, which greatly simplifies the practical realization. The tandem-NN is used to address the hard-to-converge issue caused by the non-uniqueness phenomenon that widely exists in the EM inverse problem [27]. We collect the simulation data by the finite-element method analysis software COMSOL Multiphysics and train the network-NN with the open-source high-level deep learning application programming interface (API) Keras, with an accuracy of 86.6% and 86.5% for near and far fields, respectively. The pretrained T-NN can work for a customer-desired optical response, e.g., invisibility cloak, in one single forward computation. Our work provides a new avenue to realize a transparent cloak, distinct from conventional reflected metasurface cloaks. Also, the T-NN can inspire the inverse design of other metadevices [20,31,32].

2. RESULTS

Architecture of the transmitted metasurfaces invisibility cloak. As schematically shown in Fig. 1, our proposed transmitted metasurface cloak is easy yet viable, just consisting of two planar metasurfaces, i.e., metasurface 1 (left) and metasurface 2 (right). At the top and bottom sides, two perfect electric conductor (PEC) blocks are arranged to form a closed rectangular box to prevent EM waves from scattering in other directions. Inside the rectangular box, we assume there is a dielectric cat model with the relative permittivity of 3.5, which can also be generally replaced by other objects with different shapes and materials. For conceptual clarity, we assume the transparent cloak works for the transverse magnetic (TM) plane wave excited from the left side and at 8 GHz in two dimensions. Each metasurface is composed of eight subwavelength metasurface elements (with a width of 20 mm). Here, to accelerate the simulation and data collection process, we mimic the metasurface element by setting a transition boundary condition on the section line of its position. A metasurface element is enabled to provide a continuous local transmitted spectrum shift (0 to 2π) with unitary transmission. To characterize the cloaking performance, we consider both near-field distribution (the out-of-plane magnetic field inside the rectangle region enclosed by the green dashed line) and far-field radar cross section (RCS). By modifying the metasurface properties, the near- and far-field signatures will change correspondingly. Ideally, after passing through the layered metasurfaces, the forward and backward scattering of the incident wave shall be very small, as though the rectangular box were transparent.

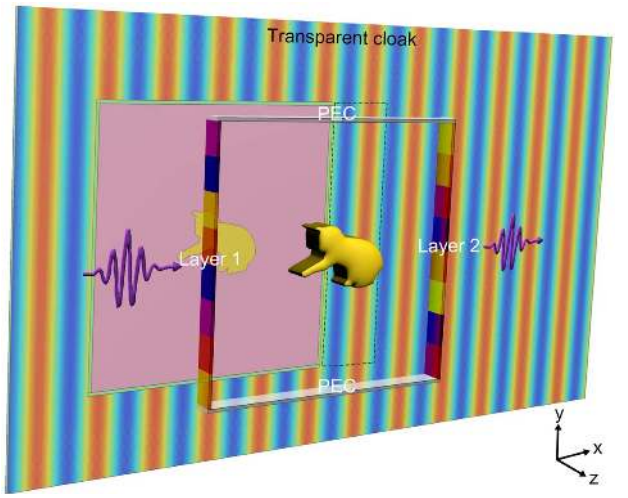

Fig. 1. Schematic of the transmitted metasurface cloak. The transmitted metasurface cloak consists of two planar metasurfaces, labelled as layer 1 and layer 2, to hide an object inside, such as a cat. Each metasurface is composed of eight subwavelength metasurface elements, each of which provides a local transmitted spectrum shift. To prevent EM waves from scattering in other directions, two PEC blocks are arranged to form a closed rectangular box. Here, we consider both near-field distribution (the out-of-plane magnetic field inside the rectangular region enclosed by the green dashed line) and far-field radar cross section to characterize the cloaking performance. Ideally, after passing through the two-layer metasurfaces, the forward and backward scattering of the incident wave shall be very small, as though the rectangular box were transparent.

Nonuniqueness issue and T-NN. Evidently, our goal is to exploit and generalize the intricate inverse relationship between the near field/far field and the transmitted spectrum of metasurface using a deep neural network. However, there is a great challenge in training the deep neural network because of the existing nonuniqueness issue in the inverse design. To be specific, the same EM field response F can be generated by multiple different metasurface arrangements S. As showcased in Fig. 2(a), two different metasurface arrangements lead to exactly the same far field and near field. This nonunique $F \rightarrow S$ will induce conflicting training samples, such as (F, S^A) and (F, S^B) in Fig. 2(a). Therefore, in the training process, the inverse neural network will encounter the serious hard-to-converge problem because the buildup data set will inevitably contain some cases having different output labels, but with the same input.

To overcome this nonunique issue, we deploy a T-NN, as shown in Fig. 2(b). The T-NN consists of two deep neural networks, i.e., an inverse neural network (termed NN1) and a forward neural network (termed NN2). For a customer-desired EM response F, the NN1 will generate a candidate of the metasurface arrangement S, and then feed S into the NN2 to predict the EM response F'. According to the uniqueness principle of electromagnetism, for the NN2, each kind of input S

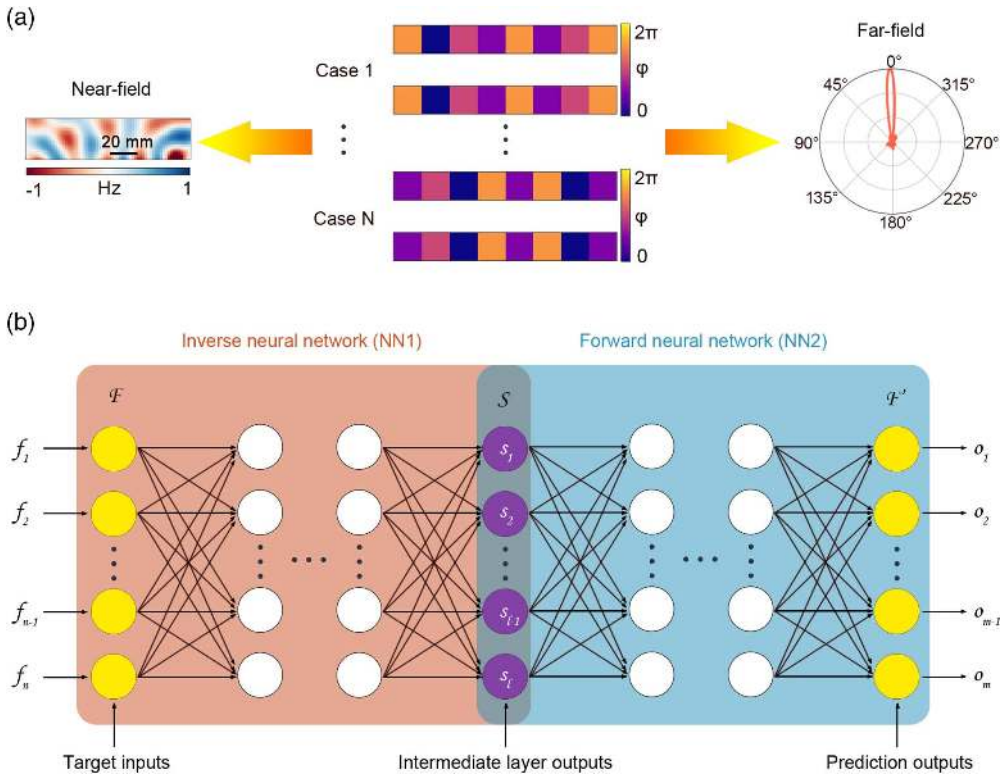

Fig. 2. Nonuniqueness issue addressed by a T-NN in the inverse design. (a) Different metasurface arrangements induce exactly the same near field and far field, called the nonuniqueness issue. This nonuniqueness issue will make the deep neural network difficult to converge. (b) Schematic of a T-NN, consisting of an inverse deep neural network (NN1) and a forward deep neural network (NN2). The NN1 has the input of near-/far-field response and the output of metasurface arrangement (nonuniqueness). In contrast, the NN2 has the input of metasurface arrangement and the output of near-/far-field response (uniqueness). In the training procedure of the T-NN, the NN2 is pretrained and fixed, and only the NN1 is updated to reduce the loss function, that is, the difference between the target field response F and the output F'. Therefore, the metasurface arrangement S can be extracted from the intermediate layer.

will only induce one unique and deterministic output, distinct from the NN1. The T-NN takes the difference between the input F and the NN2's output F' to calculate the loss function, and then iteratively updates the network. Once the T-NN is well trained, the predicted structural parameter S can be extracted from the intermediate layer output. In practice, we intend to obtain the metasurface arrangement with a customer-desired EM field response. Therefore, the T-NN can meet our practical demand and effectively address the hard-to-converge problem.

Training and evaluation of the T-NN. Before inversely designing the transparent cloak, we should consider how to build up the data set, train the T-NN, and evaluate them. To simplify the process, we only consider transmitted phase modulation while keeping the amplitudes uniform and unity (which can be accessible with current metasurface technology). Therefore, in our bilayer metasurface system, 16 metasurface elements correspond to 16 transmitted phases, each of which can be freely tuned from 0 to 2π, with a minimum precision of 0.01π. The random data of the whole phase distribution are generated step by step, i.e., we first construct some data seeds with a larger phase difference, and then use smaller phase difference to further generate data based on these seeds, so as to obtain better data distribution. The randomly generated structural parameters are imported into the simulation software, generating a great number of far-field and near-field data. In total, a data set with 200,000 samples is built up, among which 70%, 20%, and 10% are used as the training, validation, and test set.

Before training the T-NN, the forward neural network, i.e., NN2, must be trained in advance, because of the one-to-one correspondence between the input S and the output F'. After optimization, the NN2 architecture is set to have seven hidden layers for the far field (five hidden layers for near field), and each layer has 1024 neurons. The input layer has 361 neurons (discretizing the elevation angle $0-2\pi$ into 361 points) for the far field, and 1024 neurons (converting field distribution into 16×64 image pixel matrix) for the near field.

Figure 3 plots the training results of the NN2, where the loss function gradually converges, and ultimately, the accuracy at the test set reaches 85.7% (89.0%) for the far field (near field). To intuitively show the training performance, we blindly take three samples from the test set [Fig. 3(c)], and predict the EM field responses by the pretrained NN2 [green line in Fig. 3(d)]. As a comparison, we also import the input metasurface arrangements into the commercial numerical software COMSOL to obtain the EM response [ground truth, red line in Fig. 3(d)]. Each group of far-field images in Fig. 3(d) [as well as in Fig. 4(c)] is processed by a uniform normalization to better

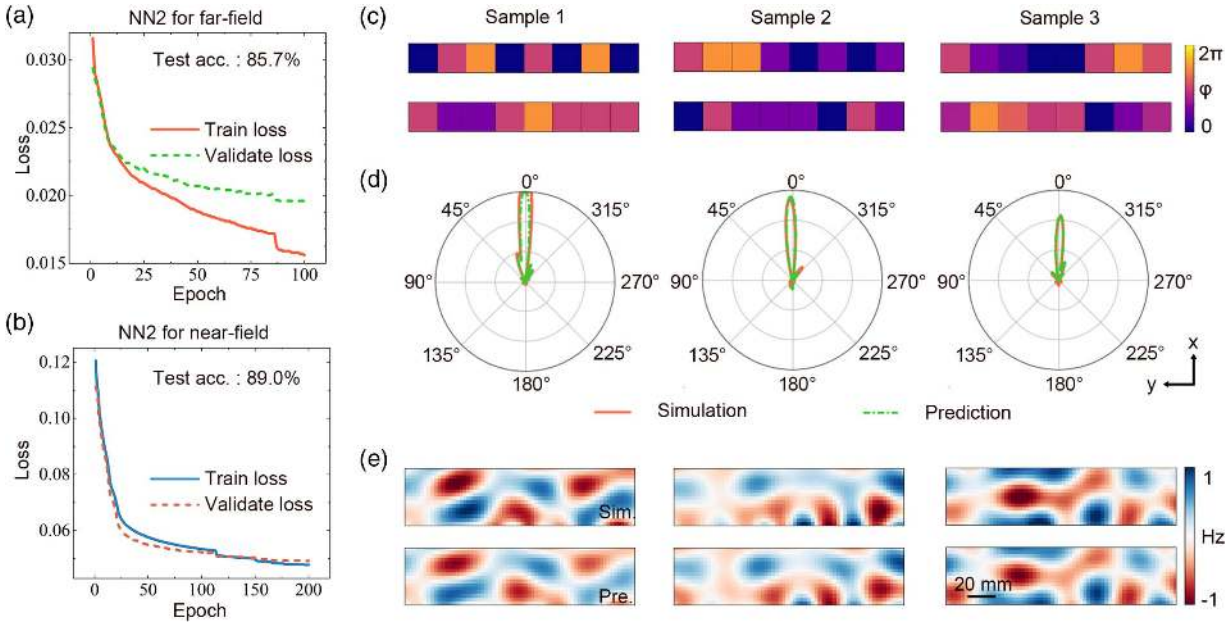

Fig. 3. Training results of the forward deep neural network (NN2). (a) Learning curve of the NN2 for the far field, with an accuracy of 85.7%; (b) learning curve of the NN2 for the near field, with an accuracy of 89.0%; (c) three metasurface arrangement samples, taken from the test set, to illustrate the performance of the NN2; (d) normalized RCS predicted by the NN2 and the simulated one obtained by importing the above three samples into the commercial numerical software COMSOL; (e) near-field distributions predicted by the NN2, and the simulated one obtained by numerical simulation.

show the result match. As shown in Figs. 3(d) and 3(e), the predicted field patterns and the ground truths are highly consistent with each other, laying a foundation for the following training of the T-NN.

With the successful training of the NN2, we next connect it to the NN1 to form a complete T-NN [Fig. 2(b)]. After optimizing, the NN1 architecture is set to have eight hidden layers (seven 1024-neuron layers plus one 512-neuron layer) for the far field, and five 1024-neuron hidden layers for the near field. It is worth noting that, in this process, the NN2 is fixed and does not participate in the parameter updating. The EM field response $F = [f_1, f_2, \cdots, f_{361}]$ for the far field and $F = [f_1, f_2, \cdots, f_{1024}]$ for the near field is separately taken as the input to train the T-NN. As mentioned above, the training aims to minimize the loss function, defined as the mean absolute error (MAE) between F and F'. Figures 4(a)–4(c) are the training results for the far field, and Figs. 4(d)–4(f) are the training results for the near field. With the decrease of the loss function [Fig. 4(a)], the test accuracy achieves 93.2%. We utilize three samples to intuitively demonstrate the training result. Figure 4(c) exhibits three types of EM field response. Type 1 is the target RCS [red curve in Fig. 4(c)]. Type 2 is the output EM field response generated by the T-NN [green curve in Fig. 4(c)], with the intermediate output metasurface arrangements S in Fig. 4(b). Type 3 is the numerical simulation of the S from the intermediate layer output [purple curve in Fig. 4(c)], which is presented as a comparison with Type 1 and Type 2. The three types of normalized RCS are drawn with the same coordinates as in Fig. 4(c), which match well with each other. For the near field [Fig. 4(d)], the loss function of the T-NN also reduces significantly, and the accuracy of the test set reaches 92.4%. Similar to the far field, we consider three samples. The target magnetic fields are plotted in the upper panel of Fig. 4(f), the output magnetic fields from the T-NN are plotted in the middle panel of Fig. 4(f), and the simulated magnetic fields are plotted in the lower panel of Fig. 4(f). These samples validate that the tandem network has a strong generality, capable of working for a customer-desired EM response.

Transparent invisibility cloak designed by the T-NN. Based on the pretrained T-NN, we progress to utilize bilayer metasurfaces to realize a transparent invisibility cloak. We input the target far field and target near field into our T-NN to predict the metasurface arrangements. After a fast calculation, we get the desired transmitted phase φ arrangement shown in Fig. 5(a). Figure 5(b) clearly demonstrates that the RCS is significantly reduced in the forward direction when the invisibility cloak is present, in stark contrast to that without the cloak. More intuitively, regarding the near-field distribution, our bared cat-shaped object leads to a strong shadow in Fig. 5(c), while the scattered field is well reconstructed in Fig. 5(d). This way, our bilayer metasurface designed by the T-NN is able to achieve excellent transparency. Whereas our transparent cloak is specifically designed at 8 GHz, the simulation results show its working bandwidth ranges from about 7.5 to 9 GHz.

Other functionalities designed by the T-NN. In addition to the transparent invisibility cloak, the pretrained T-NN metasurfaces can also be used to meet many other user-oriented demands. As an example, we utilize the advances of the T-NN metasurfaces to mimic the EM characteristic of another object, for example, a pigeon or seahorse. To reach this goal, we firstly simulate the pigeon or seahorse model (with a relative

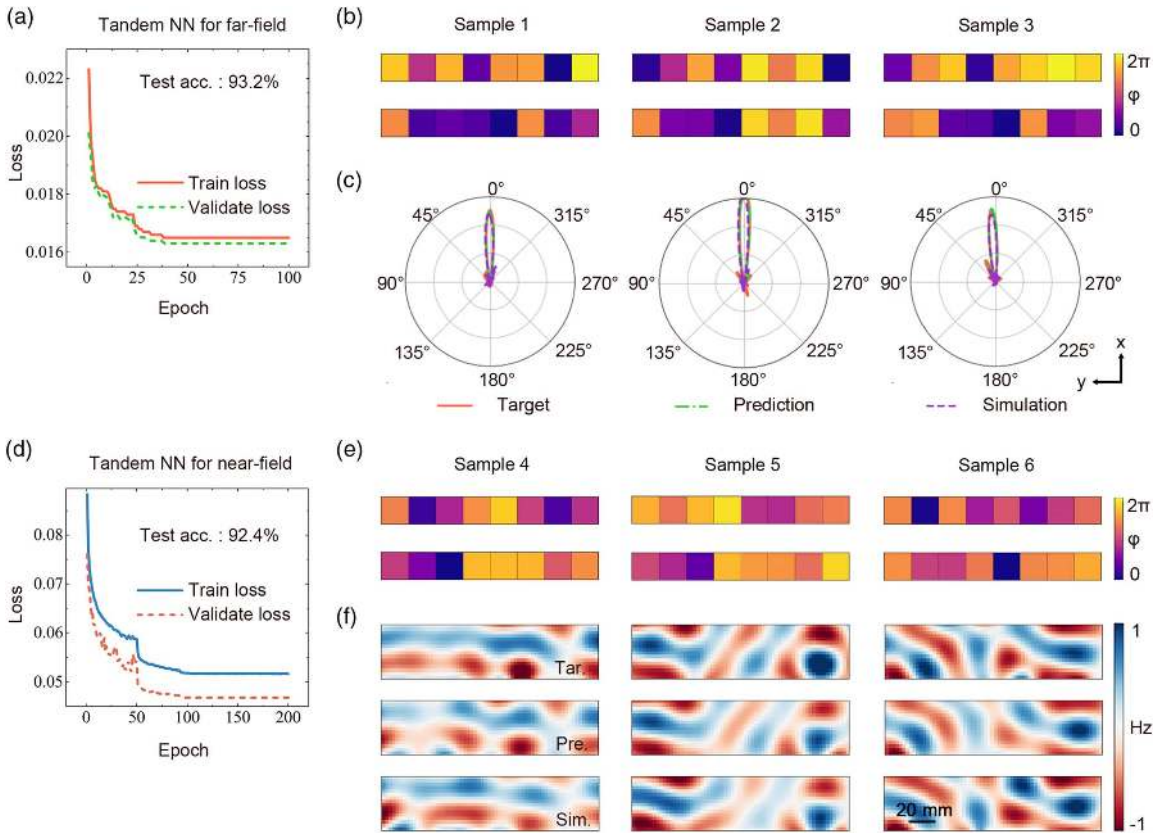

Fig. 4. Training results of the T-NN. (a) Learning curve of the T-NN for the far field, with an accuracy of 93.2%. To intuitively demonstrate the T-NN performance, we blindly select three RCS curves in the test set as the inputs [red curve in (c)], and output the metasurface arrangements from the intermediate layer, as shown in (b). In (c), we also plot the output of the T-NN (green curve), and the simulation result (purple curve) of the samples in (b). (d) Learning curve of the T-NN for the near field, with an accuracy of 92.4%; similar to the RCS above, we also blindly select three samples [upper part of (f)] as the inputs, and output the metasurface arrangements from the intermediate layer, as shown in (e). In (f), the output of the T-NN [middle part of (f)] and the simulation results [lower part of (f)] are also plotted. Obviously, these three in (f), as well as those in (c), are highly consistent with each other.

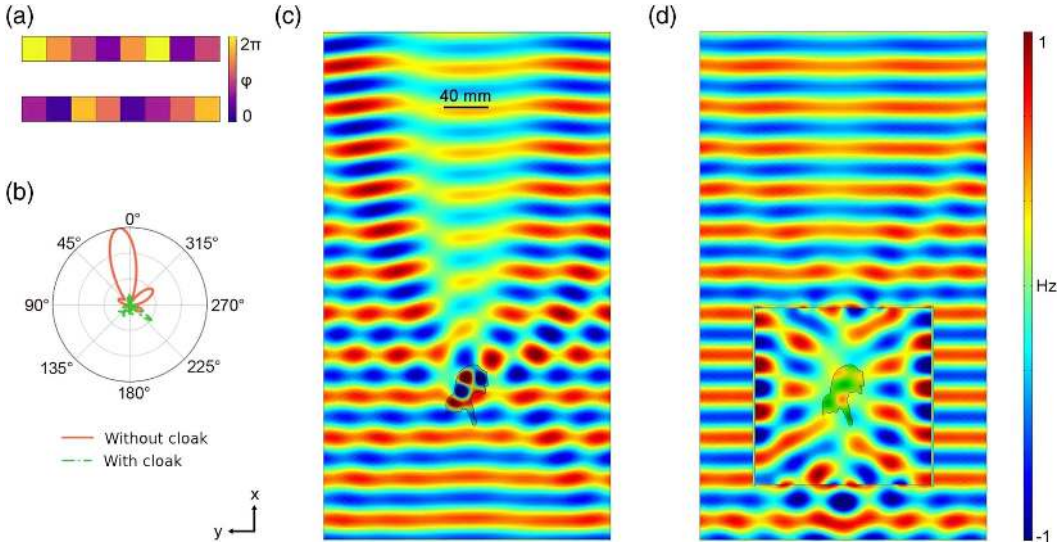

Fig. 5. Transparent invisibility cloak enabled by the pretrained T-NN. In an ideal case, the scattering of the transparent invisibility cloak should be zero, which is fed into the pretrained T-NN as the input. As such, we obtain the metasurface arrangements in (a). Based on (a), we obtain the normalized RCS of the dielectric cat with/without the cloak, as shown in (b). (c) and (d) are the simulated magnetic fields without/with the cloak, respectively, where the incident plane wave propagates from bottom to top. In (d), the field keeps almost flat after passing though the cloaking device, in stark contrast to that in (c).

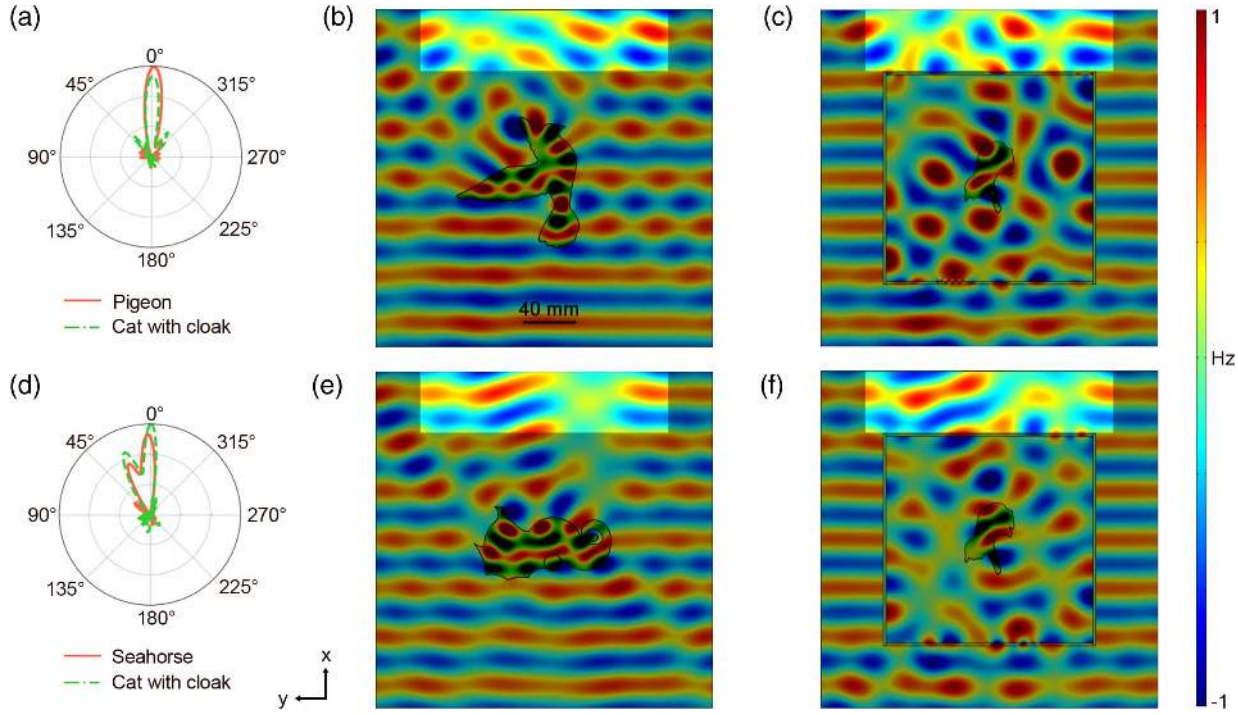

Fig. 6. Other functionalities enabled by T-NN. (a) Normalized RCS of a dielectric pigeon and a dielectric cat surrounded by a bilayer metasurface; (b), (c) simulated magnetic field distribution of (b) the pigeon and (c) the cat with a bilayer metasurface; (d) normalized RCS of a dielectric seahorse and a dielectric cat with a bilayer metasurface; (e), (f) simulated magnetic field distribution of (e) the seahorse and (f) the cat with a bilayer metasurface.

permittivity of 3.5), and input the simulated far-field response [red lines in Figs. 6(a) and 6(d)] and near-field response [highlighted regions in Figs. 6(b) and 6(e)] into the pretrained T-NN. Then, according to the output of the T-NN, we resimulate the designed bilayer metasurface cloaks, as shown in Fig. 6. The high consistency between the ground truths and the T-NN predicted results suggests that our T-NN metasurfaces are generalized and applicable for different purposes.

3. CONCLUSION

In conclusion, we proposed an easy yet viable approach to realizing the transmitted metasurface cloak, and introduced a T-NN to efficiently streamline the inverse design process. The transmitted metasurfaces cloak hides a cat-shaped object sandwiched between two planar metasurfaces. The T-NN is deployed to address the hard-to-converge issue caused by the nonuniqueness phenomenon that widely exists in the EM inverse problem. Once pretrained, the T-NN can work for a customer-desired optical response in one single forward computation, including an invisibility cloak. Our work opens a new pathway to realizing a transparent cloak and enables a variety of other applications [20,33,34].

Funding. National Natural Science Foundation of China (11961141010, 61625502, 61975176, 61975182, 62071424); Top-Notch Young Talents Program of China; Fundamental Research Funds for the Central Universities.

Acknowledgment. C. Q., B. Z., and H. C. conceived the idea for this research. Z. Z. performed the simulation and built the neural network model. Z. Z. and C. Q. wrote the paper. Y. J. and Z. F. provided help with the deep neural network. E. L., R. H., T. C., B. Z., and H. C. shared their insights and contributed to discussions on the results. C. Q., R. H., H. C., and B. Z. supervised the project.

Disclosures. The authors declare no competing financial interests.

Data availability. The data that support the findings of this study are available from the authors upon reasonable request.

REFERENCES

1. N. Engheta and R. W. Ziolkowski, *Metamaterials: Physics and Engineering Explorations* (Wiley, 2006).
2. J. B. Pendry, D. Schurig, and D. R. Smith, "Controlling electromagnetic fields," Science **312**, 1780–1782 (2006).
3. D. Schurig, J. J. Mock, B. J. Justice, S. A. Cummer, J. B. Pendry, A. F. Starr, and D. R. Smith, "Metamaterial electromagnetic cloak at microwave frequencies," Science **314**, 977–980 (2006).
4. Y. Lai, J. Ng, H. Y. Chen, D. Z. Han, J. J. Xiao, Z. Q. Zhang, and C. T. Chan, "Illusion optics: the optical transformation of an object into another object," Phys. Rev. Lett. **102**, 253902 (2009).
5. H. Y. Chen, C. T. Chan, and P. Sheng, "Transformation optics and metamaterials," Nat. Mater. **9**, 387–396 (2010).
6. Q. Chao, R. Li, Y. Jiang, B. Zheng, H. Wang, Z. Xu, and H. Chen, "Transient response of a signal through a dispersive invisibility cloak," Opt. Lett. **41**, 4911–4914 (2016).

7. B. Zheng, R. Zhu, L. Jing, Y. Yang, and H. Chen, "3D visible-light invisibility cloak," Adv. Sci. **5**, 1800056 (2018).
8. N. Yu, P. Genevet, M. A. Kats, and F. Aieta, "Light propagation with phase discontinuities: generalized laws of reflection and refraction," Science **334**, 333–337 (2011).
9. S. Sun, Q. He, S. Xiao, Q. Xu, X. Li, and L. Zhou, "Gradient-index meta-surfaces as a bridge linking propagating waves and surface waves," Nat. Mater. **11**, 426–431 (2012).
10. T. J. Cui, M. Q. Qi, X. Wan, Z. Jie, and C. Qiang, "Coding metamaterials, digital metamaterials and programmable metamaterials," Light Sci. Appl. **3**, e218 (2014).
11. T. Cai, G. M. Wang, S. W. Tang, H. X. Xu, J. W. Duan, H. J. Guo, F. X. Guan, S. L. Sun, Q. He, and L. Zhou, "High-efficiency and full-space manipulation of electromagnetic wave fronts with metasurfaces," Phys. Rev. Appl. **8**, 034033 (2017).
12. T. Cai, S. Tang, G. Wang, H. Xu, S. Sun, Q. He, and L. Zhou, "High-performance bifunctional metasurfaces in transmission and reflection geometries," Adv. Opt. Mater. **5**, 1600506 (2017).
13. C. Qian, X. Lin, Y. Yang, X. Xiong, H. Wang, E. Li, I. Kaminer, B. Zhang, and H. Chen, "Experimental observation of superscattering," Phys. Rev. Lett. **122**, 063901 (2019).
14. L. Li, H. Ruan, C. Liu, Y. Li, Y. Shuang, A. Alù, C. Qiu, and T. Cui, "Machine-learning reprogrammable metasurface imager," Nat. Commun. **10**, 1082 (2019).
15. C. Qian, X. Lin, X. Lin, J. Xu, Y. Sun, E. Li, B. Zhang, and H. Chen, "Performing optical logic operations by a diffractive neural network," Light Sci. Appl. **9**, 59 (2020).
16. X. Ni, Z. J. Wong, M. Mrejen, Y. Wang, and X. Zhang, "An ultrathin invisibility skin cloak for visible light," Science **349**, 1310–1314 (2015).
17. J. Zhang, Z. L. Mei, W. R. Zhang, Y. Fan, and T. J. Cui, "An ultrathin directional carpet cloak based on generalized Snell's law," Appl. Phys. Lett. **103**, 151115 (2013).
18. B. Orazbayev, N. M. Estakhri, M. Beruete, and A. Alu, "Terahertz carpet cloak based on a ring resonator metasurface," Phys. Rev. B **91**, 195444 (2015).
19. H. Lu, B. Zheng, T. Cai, C. Qian, Y. Yang, Z. Wang, and H. Chen, "Frequency-controlled focusing using achromatic metasurface," Adv. Opt. Mater. **9**, 2001311 (2020).
20. C. Qian, B. Zheng, Y. Shen, L. Jing, E. Li, L. Shen, and H. Chen, "Deep-learning-enabled self-adaptive microwave cloak without human intervention," Nat. Photonics **14**, 383–390 (2020).
21. H. Chu, Q. Li, B. Liu, J. Luo, S. Sun, Z. Hang, L. Zhou, and Y. Lai, "A hybrid invisibility cloak based on integration of transparent metasurfaces and zero-index materials," Light Sci. Appl. **7**, 50 (2018).
22. H. Li, M. Rosendo-López, Y. Zhu, X. Fan, D. Torrent, B. Liang, J. Cheng, and J. Christensen, "Ultrathin acoustic parity-time symmetric metasurface cloak," Research **2019**, 8345683 (2019).
23. Z. C. Liu, D. Y. Zhu, S. P. Rodrigues, K. Lee, and W. Cai, "Generative model for the inverse design of metasurfaces," Nano Lett. **18**, 6570–6576 (2018).
24. W. Ma, F. Cheng, and Y. M. Liu, "Deep-learning-enabled on-demand design of chiral metamaterials," ACS Nano **12**, 6326–6334 (2018).
25. S. Molesky, Z. Lin, A. Y. Piggott, W. Jin, J. Vucković, and A. W. Rodriguez, "Inverse design in nanophotonics," Nat. Photonics **12**, 659–670 (2018).
26. J. Peurifoy, Y. Shen, L. Jing, Y. Yang, F. Cano-Renteria, B. G. DeLacy, J. D. Joannopoulos, M. Tegmark, and M. Soljačić, "Nanophotonic particle simulation and inverse design using artificial neural networks," Sci. Adv. **4**, eaar4206 (2018).
27. D. Liu, Y. Tan, E. Khoram, and Z. Yu, "Training deep neural networks for the inverse design of nanophotonic structures," ACS Photon. **5**, 1365–1369 (2018).
28. L. Gao, X. Li, D. Liu, L. Wang, and Z. Yu, "A bidirectional deep neural network for accurate silicon color design," Adv. Mater. **31**, 1905467 (2019).
29. Y. Long, J. Ren, Y. Li, and H. Chen, "Inverse design of photonic topological state via machine learning," Appl. Phys. Lett. **114**, 181105 (2019).
30. W. Ma, Z. Liu, Z. A. Kudyshev, A. Boltasseva, W. Cai, and Y. Liu, "Deep learning for the design of photonic structures," Nat. Photonics **15**, 77–90 (2020).
31. F. Liu, O. Tsilipakos, A. Pitilakis, A. C. Tasolamprou, M. S. Mirmoosa, N. V. Kantartzis, D. Kwon, J. Georgiou, K. Kossifos, M. A. Antoniades, M. Kafesaki, C. M. Soukoulis, and S. A. Tretyakov, "Intelligent metasurfaces with continuously tunable local surface impedance for multiple reconfigurable functions," Phys. Rev. Appl. **11**, 044024 (2019).
32. O. Tsilipakos, A. C. Tasolamprou, A. Pitilakis, F. Liu, X. Wang, M. S. Mirmoosa, D. C. Tzarouchis, S. Abadal, H. Taghvaee, C. Liaskos, A. Tsioliaridou, J. Georgiou, A. Cabellos-Aparicio, E. Alarcón, S. Ioannidis, A. Pitsillides, I. F. Akyildiz, N. V. Kantartzis, E. N. Economou, C. M. Soukoulis, M. Kafesaki, and S. Tretyakov, "Toward intelligent metasurfaces: the progress from globally tunable metasurfaces to software-defined metasurfaces with an embedded network of controllers," Adv. Opt. Mater. **8**, 2000783 (2020).
33. C. Qian, H. Wang, R. Li, B. Zheng, Z. Xu, and H. Chen, "Observing the transient buildup of a superscatterer in the time domain," Opt. Express **25**, 4967–4974 (2017).
34. S. Xu, F. Dong, W. Guo, D. Han, C. Qian, F. Gao, W. Su, H. Chen, and H. Sun, "Cross-wavelength invisibility integrated with various invisibility tactics," Sci. Adv. **6**, eabb3755 (2020).